Available online at www.sciencedirect.com
SCIENCE DIRECT®
Journal of Solid State Chemistry 177 (2004) 1738–1745
JOURNAL OF SOLID STATE CHEMISTRY
http://elsevier.com/locate/jssc

Synthesis, properties and structure determination of $Nb_2O_3(SO_4)_2 \cdot \frac{1}{4}H_2O$ from neutron and synchrotron X-ray powder diffraction data

Magnus Boström,[a,*] Mauro Gemmi,[b] Walter Schnelle,[c] and Lars Eriksson[a]

[a] Department of Structural Chemistry, Stockholm University, Stockholm 10691, Sweden
[b] Dipartimento di Scienze della Terra "Ardito Desio", Università di Milano, via Botticelli 23, Milano 20133, Italy
[c] Max-Planck-Institut für Chemische Physik fester Stoffe, Nöthnitzer Straße 40, Dresden 01187, Germany

Received 15 October 2003; received in revised form 22 December 2003; accepted 30 December 2003

Abstract

The blue diamagnetic compound $Nb_2O_3(SO_4)_2 \cdot \frac{1}{4}H_2O$ was synthesized by reaction of niobium metal and boiling sulfuric acid. The unit cell was deduced from electron diffraction patterns and the crystal structure was solved from X-ray powder diffraction data and refined from combined X-ray synchrotron and neutron powder diffraction data. $Nb_2O_3(SO_4)_2 \cdot \frac{1}{4}H_2O$ crystallizes in the space group $R\bar{3}$ (148) with the cell parameters $a = 10.384(2)$ Å and $c = 26.55(2)$ Å in the hexagonal setting. The structure features covalently bonded sulfate tetrahedra and niobate octahedra.

Keywords: Oxysulfate; Oxide sulfate; Crystal structure; Rietveld refinement

1. Introduction

Predominately the high oxidation number and high electronegativity, resulting in a small ionic radius, prevent niobium from forming typical sulfate salts. Instead, niobium (+V) forms oxysulfates of the type $Nb_2O_x(SO_4)_{5-x}$. In aqueous solution only compounds with $x = 3$ and 4 are formed [1].

There are no known examples of oxysulfates built up from three-dimensional networks of apex sharing sulfate tetrahedra and $[MO_6]^{n+}$ octahedra centred by M = Nb. However, many examples exist where the metal M is Ti, Zr or V. These show a rich variety of structures where the metal octahedra are connected forming clusters [2,3], chains [4–10], pairs [11] or occur isolated [12,13]. The sulfate tetrahedra connect these octahedra units to complete the three-dimensional network. Nb occurs in similar structures in oxyphosphates [14–20]. $Nb_2O_3(SO_4)_2$ is known to exist in two modifications, a white and a blue one. The white modification is synthesized by dissolving Nb_2O_5 in boiling concentrated H_2SO_4. It has been reported to transform to the blue modification upon heating at temperatures less than 500°C [21].

The present paper communicates a direct synthesis route to blue $Nb_2O_3(SO_4)_2 \cdot \frac{1}{4}H_2O$, its properties and its crystal structure. To our knowledge, this is the first determined structure of a niobiumoxysulfate.

2. Experimental

2.1. Synthesis

A beaker containing 200 cm^3 concentrated sulfuric acid was added 2.0 g powdered niobium metal. No reaction could be observed until the sulfuric acid was heated to boiling temperature. At this temperature, the niobium metal reacted with the sulfuric acid under evolution of a yellow-brown gas and formation of a blue precipitate. Additionally, some yellow spherical sulfur particles were observed. The blue precipitate was subsequently separated from the mother liquid by vacuum filtering through a glass funnel fitted with a sintered glass filter. The precipitate was dried by the airflow through the funnel and subsequently washed with ethanol and later distilled water. It was imperative that the precipitate was essentially free from mother

*Corresponding author. Fax: +46-8-163118.
E-mail address: bostroem@cpfs.mpg.de (M. Boström).

0022-4596/$ - see front matter © 2004 Elsevier Inc. All rights reserved.
doi:10.1016/j.jssc.2003.12.035

liquid before the water was added, otherwise a white gelatinous precipitate immediately formed as impurity. Several batches were made to avoid the handling of large volumes of boiling concentrated sulfuric acid.

A sample free of sulfur and unreacted niobium metal was necessary for the DTA/TG and magnetization measurement. Removal of these two impurities was carried out by making a slurry of the raw product in water, allowing the larger niobium and sulfur particles to sediment and then decanting the liquid containing the finely dispersed $Nb_2O_3(SO_4)_2 \cdot \frac{1}{4}H_2O$ particles. The water was evaporated at 120°C.

2.2. Electron diffraction

A specimen for electron microscopy was prepared by grinding the sample in an agate mortar together with isopropanol and deposition of it on a copper grid with a holey carbon film. The electron diffraction study was carried out with a JEOL 2000FX electron microscope operating at 200 kV.

2.3. Powder diffraction

Conventional laboratory X-ray powder diffraction data were collected using Cu$K\alpha_1$ radiation with a STOE STADI/P powder diffractometer in the 2θ-range from 8.00° to 120.0° with a step length of 0.02°. After correction for the zero point error, these data were used for the structure solution with the EXPO program [22,23]. The unit cell was refined from data collected at room temperature with a HUBER Image Plate Guiner camera using Cu$K\alpha_1$ radiation. The unit cell was refined with the CELLREF program [24]. Cell refinement data were also collected after heating as-synthesized samples at 150°C (38 h), 200°C (15 h), 350°C (12 h), 400°C (508 h), 500°C (22 h) and 550°C (67 h). The sample annealed at 350°C was immersed in distilled water at ambient conditions during 7 months after the annealing. Cell refinement data were collected after the sample had been dried at room temperature. Silicon powder was added to all samples used for cell refinement as internal standard.

Neutron diffraction was carried out at the Studsvik Neutron Research Laboratory in Sweden. The neutron diffraction pattern was measured from 4° to 140° in 2θ with an angular increment of 0.080°.

Synchrotron X-ray diffraction was carried out at the ID31 beam line of ESRF in Grenoble, France. Data were collected from 3° to 49° with a wavelength of 0.496 Å. The data reduction was performed with an angular increment of 0.003°.

The final refinement was carried out simultaneously on neutron and synchrotron data with the program GSAS [25] with the crystal structure refined from X-ray laboratory data as starting model.

2.4. Bond-valence calculation

Bond-valence calculations were performed with the CHARDIS99 program [26], using the bond distances obtained from the refinement and the Brown–Altermatt parameters [27].

2.5. Magnetization measurements

Magnetization measurements were performed at external fields between 70 kOe and 100 Oe in the temperature range 1.8–320 K in a SQUID (Quantum Design MPMS-XL7) magnetometer.

2.6. TGA/DTA

DTA/TG data were collected in the range 25–1400°C with the heating rate 10 K/min using a NETZSCH STA409 instrument. The sample was kept in a alumina crucible in air.

3. Results

3.1. Structure refinement

Electron diffraction data showed that $Nb_2O_3(SO_4)_2 \cdot \frac{1}{4}H_2O$ has a rhombohedrally distorted face centred cubic lattice. The refined unit cell parameters in the hexagonal setting are $a = 10.384(2)$ Å and $c = 26.55(2)$ Å. Electron diffraction patterns of the fundamental projections of the pseudocubic lattice are shown in Fig. 1. The rhombohedral distortion of the unit cell from cubic face centred is rather slight, and the unconventional face centred rhombohedral cell has the rhombohedral angle $\alpha = 88.33(1)°$.

The structure model derived with direct methods features a three-dimensional network of corner sharing

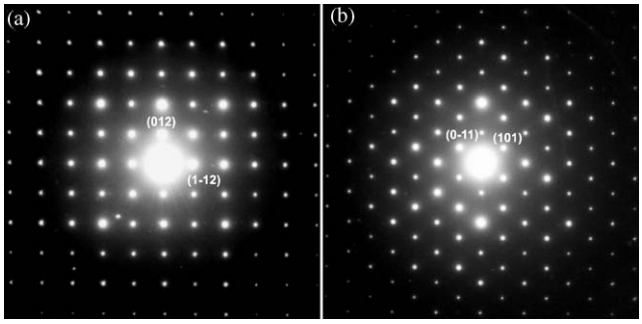

Fig. 1. Selected area electron diffraction patterns of $Nb_2O_3(SO_4)_2 \cdot \frac{1}{4}H_2O$. The indices are given with respect to the hexagonal unit cell. (a) $[42\bar{1}]$ projection corresponding to the fundamental [100] direction in the unconventional face centred rhombohedral cell. (b) $[\bar{1}11]$ projection corresponding to the [101] direction in the unconventional face centred rhombohedral cell.

sulfate tetrahedra and niobate octahedra. The network was found to have cavities in the structure large enough to host water. Therefore, difference Fourier maps were calculated after a preliminary refinement to seek for water molecules. The neutron data difference Fourier map reveals the oxygen atom of a water molecule as a strong positive peak labeled as A in Fig. 2. A negative peak, labeled B, is located nearly halfway to the closest oxygen position O8. The negative peak and its symmetry equivalent at the opposite side of the oxygen atom were refined as half-occupied hydrogen positions. The oxygen site and the two hydrogen sites fall upon a line, and consequently, the two hydrogen atoms cannot belong to the same water molecule at any given time.

No other negative peaks could be found in the vicinity of the oxygen position labeled A. However, a diffuse negative background was observed where the other hydrogen atom was expected to be found, based on the H–O–H angle of water.

The full refinement of the complete model was carried out simultaneously on both neutron and synchrotron powder diffraction data. The neutron diffraction pattern was weighted with a factor equal to the ratio between the number of observed points in synchrotron diffraction data and neutron diffraction data (~ 10). Neutron and X-ray data had in this way the same impact on the refinement. The scale factor, the background, the profile function, the cell parameters, the coordinates and isotropic temperature parameters were refined, in total 92 parameters. The agreement factors from the Rietveld refinement were $wR_p = 0.024$, $R_p = 0.020$, $R_{Bragg} = 0.054$ for neutrons and $wR_p = 0.12$, $R_p = 0.10$, $R_{Bragg} = 0.11$ for synchrotron data. The total reduced $\chi^2 = 1.54$ (see Table 1). The refined atomic coordinates and thermal parameters are listed in Table 2. From the neutron diffraction analysis the sample was found to contain 21 wt% niobium metal. The eight reflections from the niobium metal contributed to about 1% of the total scattered intensity in the neutron pattern and did not cause any problems in the refinement. No other impurities could be observed in the neutron powder diffraction pattern. No traces of niobium were found in the sample used for the synchrotron X-ray diffraction refinement. The observed diffraction patterns, the calculated patterns and the difference curves are shown in Fig. 3.

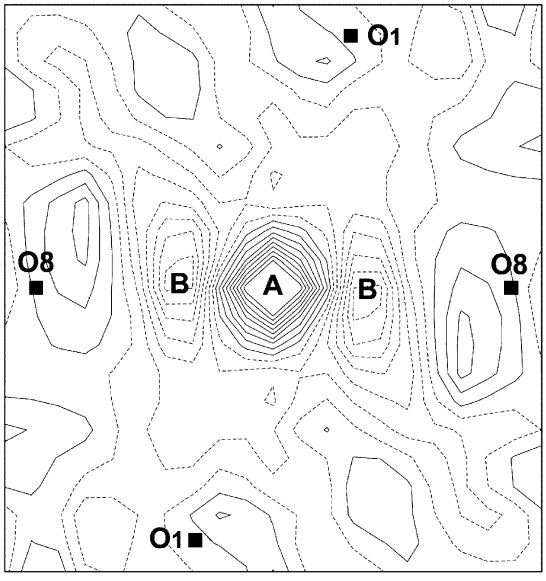

Fig. 2. Two-dimensional section of a difference Fourier map calculated on neutron data. The section has been done on the plane containing the O8 and O1 and the coordinates of the center are $(0, 0, 1/2)$. Solid and dashed lines indicate positive and negative contour levels, respectively. One strong positive peak A and two negative peaks B can be identified.

Table 1
Crystal data and refinement parameters for $Nb_2O_3(SO_4)_2 \cdot \frac{1}{4}H_2O$

Crystal data	
Chemical formula	$Nb_2O_3(SO_4)_2 \cdot \frac{1}{4}H_2O$
Unit cell dimensions (Å)*	$a = 10.384(1)$, $c = 26.55(2)$
Cell volume (Å^3)*	$V = 2479(3)$
Space Group; Z	R-3 (148); 12
Density calc. (g cm^{-3})	3.473
Color	Blue
Synchrotron X-ray	
λ (Å)	0.4956
Range of 2θ (°)	2.622–48.663
Increment 2θ (°)	0.003
Number of data points	16221
Reflections observed	2684
wR_p	0.1218
R_p	0.1006
R_{Bragg}	0.1077
Neutrons	
λ (Å)	1.4701
Range of 2θ (°)	4.0–137.92
Increment 2θ (°)	0.08
Number of data points	1675
Reflections observed	1196
wR_p	0.024
R_p	0.020
R_{Bragg}	0.054
Combined refinement	
wR_p	0.063
R_p	0.073
Reduced χ^2	1.52
GOF	1.23
Number of refined variables	94

*Refined from Guiner data with Si as internal standard.

3.2. Crystal structure description

O atoms coordinate Nb atoms octahedrally and S atoms tetrahedrally. The average Nb–O distance in the octahedra is 1.98 Å, varying in the range 1.87–2.10 Å, and the average S–O distance in the tetrahedra is 1.47 Å,

Table 2
Coordinates and thermal parameters for $Nb_2O_3(SO_4)_2 \cdot \frac{1}{4}H_2O$, as refined from combined neutron and synchrotron X-ray powder diffraction data

Atom	Wyckoff symbol	Occupancy	x	y	z	U_{iso}
Nb1	18*f*	1	0.3290(3)	0.1151(3)	0.2916(2)	0.0096(4)
Nb2	6*c*	1	2/3	1/3	0.2091(2)	0.0099(8)
S1	18*f*	1	0.1657(7)	0.2706(6)	0.2159(3)	0.010(2)
S2	6*c*	1	0	0	0.3533(4)	0.013(3)
O1	18*f*	1	0.298(2)	0.403(2)	0.1988(4)	0.020(4)
O2	18*f*	1	0.197(2)	0.173(2)	0.2478(4)	0.017(4)
O3	18*f*	1	0.370(2)	0.282(2)	0.3343(6)	0.022(5)
O4	18*f*	1	0.491(2)	0.228(2)	0.2475(4)	0.013(4)
O5	18*f*	1	0.069 (2)	0.312(2)	0.2462(5)	0.017(4)
O6	18*f*	1	0.136(2)	0.001(2)	0.3331(4)	0.013(4)
O7	18*f*	1	0.077(2)	0.181(2)	0.1717(4)	0.017(3)
O8	6*c*	1	0	0	0.4067(9)	0.035(7)
O9	3*b*	1	0	0	1/2	0.031(7)
H1	6*c*	1/2	0	0	0.463(4)	0.031(7)

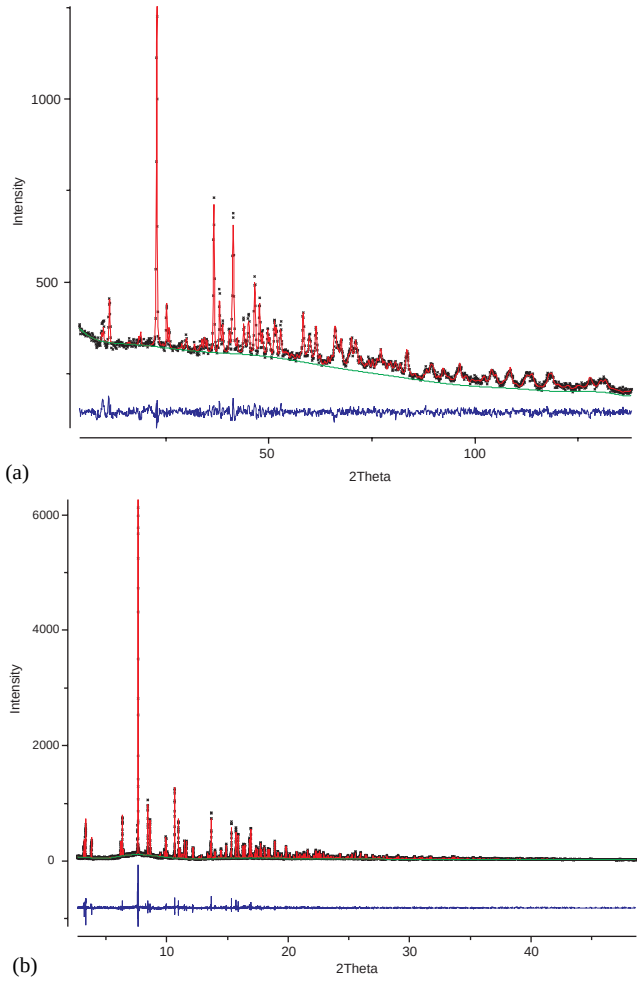

Fig. 3. (a) Observed diffraction pattern, the calculated pattern and the difference curve for the neutron powder diffraction Rietveld refinement of $Nb_2O_3(SO_4)_2 \cdot \frac{1}{4}H_2O$. (b) Observed diffraction pattern, the calculated pattern and the difference curve for the synchrotron X-ray powder diffraction Rietveld refinement of $Nb_2O_3(SO_4)_2 \cdot \frac{1}{4}H_2O$.

Table 3
Cation–oxygen distances in the Nb octahedra and S tetrahedra

Atom pair	Distance (Å)
Nb1–O3	1.88(2)
Nb1–O4	1.89(2)
Nb1–O3	1.93(2)
Nb1–O5	2.05(2)
Nb1–O6	2.06(2)
Nb1–O2	2.09(2)
Nb2–3O4	1.89(2)
Nb2–3O7	2.06(2)
S1–O1	1.45(2)
S1–O2	1.48(2)
S1–O7	1.49(2)
S1–O5	1.50(2)
S2–O8	1.42(3)
S2–3O6	1.501(9)

varying in the range 1.41–1.51 Å, see Table 3. The O–Nb–O angles in the niobium octahedra are in the range 82.8–98.9° and the O–S–O angles in the sulfate tetrahedra range from 107.5° to 113.6°.

The structure is conveniently described in terms of two approximately cubic subunits, one made up of eight apex-sharing niobate octahedra and the other made up of eight isolated sulfate tetrahedra, cf. Fig. 4. Each sulfate tetrahedron has one unshared O atom, pointing into the middle of the significantly rhombohedrally oblately distorted sulfate pseudocube. Its deviation from cubic symmetry is clearly seen in the slight rotation of the sulfate tetrahedra, cf. Fig. 4d. The sulfate pseudocube harbors one molecule of water, with its oxygen atom in the middle of the pseudocube. One of the hydrogen atoms of this water molecule forms a

hydrogen bond along the shortest pseudocube diagonal to the free oxygen atom of a sulfate tetrahedron. This hydrogen bond is parallel to the three-fold unit cell axis and the other hydrogen is dislocated on a circle, cf. Fig. 5. The hydrogen bond can form to either of the O8 atoms on opposite side of the water molecule O9 atom. Therefore, the water molecule has two possible orientations and the H1 position has half occupancy. The thermal parameters for O8 and O9 are the highest among all O atoms in the structure. This might be due to that the O8 and O9 atoms shifts very slightly depending on which of the O8 atoms are involved in the hydrogen bond.

The niobate pseudocubes have no direct contact between each other in the structure. Instead, the oxygen atoms that are not involved in Nb–O–Nb bonds within the niobate pseudocubes form Nb–O–S bonds with sulfate groups in sulfate pseudocubes. Niobate cubes are in this way linked with each other by sulfate tetrahedra, cf. Fig. 6. Every sulfate tetrahedron shares three of its oxygen atoms with niobium octahedra.

Together the niobate and sulfate pseudocubes build up the crystal structure by sharing square faces indicated by the dashed lines in Fig. 4. In this way layers parallel to {012} in the hexagonal setting are formed, cf. Fig. 6. These layers build up the whole structure by stacking. The full structure with niobate and sulfate pseudocubes as units can be seen as fully analogous to a rhombohedrally distorted NaCl structure.

The niobate and sulfate pseudocubes can be considered to build up the complete structure only by

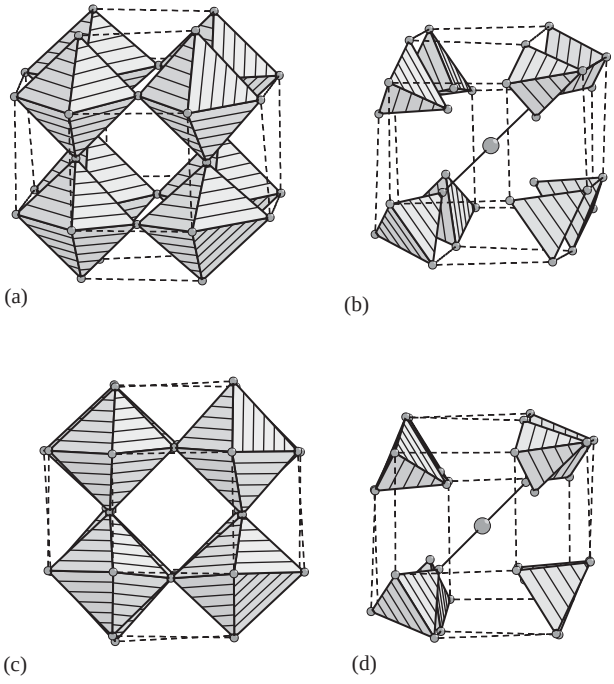

Fig. 4. (a) Niobate and (b) sulfate pseudocube-subunits slightly tilted. The square faces formed by four oxygen atoms are outlined with dashed lines. These faces are shared when these pseudocubes build up the full structure. When (c) the niobium pseudocubet and (d) the sulfate pseudocube are viewed aligned, the deviation from cubic symmetry is very clear in the case of the sulfate pseudocube.

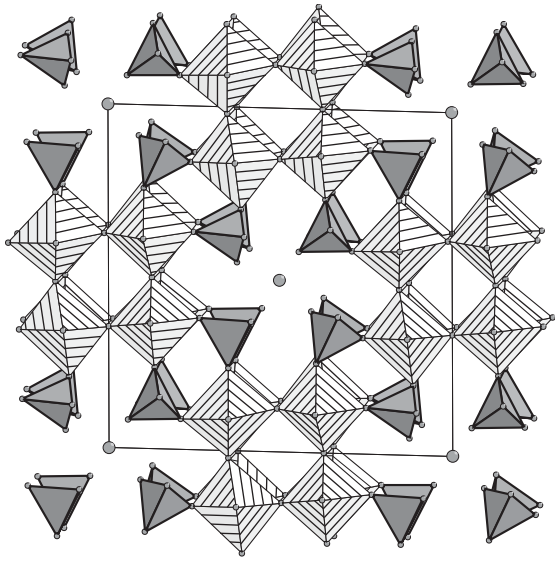

Fig. 6. One layer of connected niobate and sulfate pseudocubes. Niobate octahedra are drawn light gray and hatched. Sulfate tetrahedra and oxygen atoms are dark gray. The layer is parallel with {012} of the hexagonal cell and {100} of the unconventional face centred rhombohedral cell. The niobate pseudocubes never completely superimpose, since they are displaced by the sulfate pseudocubes.

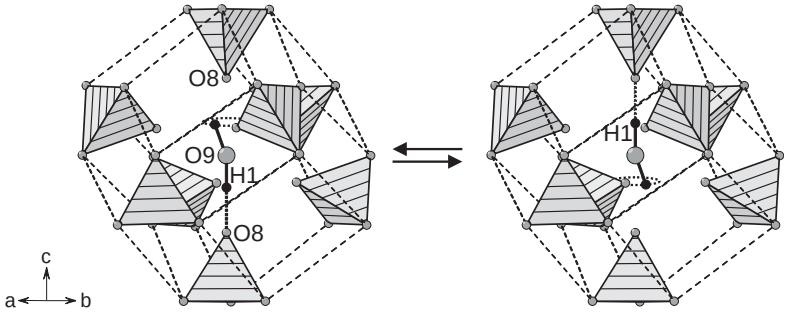

Fig. 5. The two different orientations of the water molecule in the sulfate pseudocubes. The hydrogen bond is drawn with dashed lines.

translation, without any rotation. Since the niobate pseudocube has nearly perfect cubic symmetry, the rhombohedral distortion of the sulfate pseudocube can be considered the main reason for the unit cell to be rhombohedral rather than cubic. The unconventional face centred rhombohedral unit cell and its content are shown in Fig. 7.

3.3. Bond-valence calculation

The valences of the cations obtained from the bond-valence calculation were 5.05 for Nb1, 5.21 for Nb2, 5.90 for S1 and 5.91 for S2.

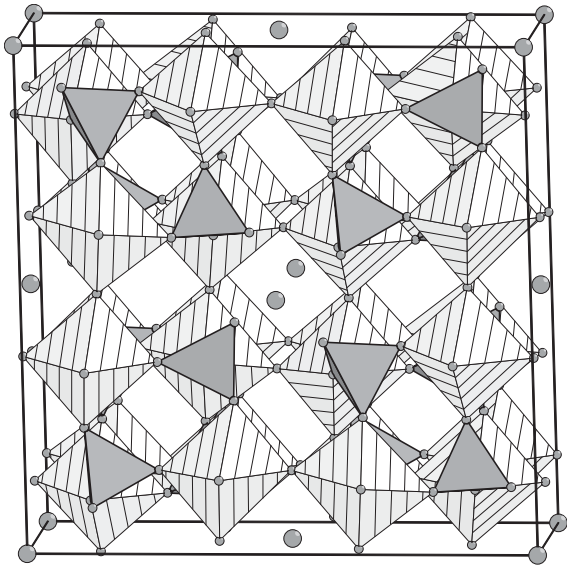

Fig. 7. Unit cell content of one unconventional rhombohedral face centred unit cell. Niobate octahedra are drawn light gray and hatched. Sulfate tetrahedra and oxygen atoms are dark gray.

3.4. Magnetization measurements

The magnetization of a powder sample of purified $Nb_2O_3(SO_4)_2 \cdot \frac{1}{4}H_2O$ showed a small paramagnetic moment (corresponding to 5.6 at% of spin $\frac{1}{2}$ species). This small amount of magnetic moments presumably stems from impurities or crystal defects while the crystalline compound itself is diamagnetic. In low fields, a strong diamagnetic signal below ca. 9.0 K signals the superconductivity of some elemental Nb ($T_c = 9.2$ K), which is present in a volume fraction of ca. 5×10^{-5} as concluded from its flux expulsion. Thus, the purified material contains only minor unreacted educts. A temperature independent term $\chi_0 = -89(10) \times 10^{-6}$ emu mol^{-1} is obtained from high field data corrected for the impurities. In comparison to the sum of the tabulated diamagnetic core contributions (-134×10^{-6} emu mol^{-1}) [27] a temperature independent paramagnetism of $+45(10) \times 10^{-6}$ emu mol^{-1} can be deduced. In conclusion, the magnetic susceptibility confirms that niobium is present in the oxidation state +V in the compound.

3.5. TGA/DTA and thermal stability

The experimental DTA/TGA curve is shown in Fig. 8. The theoretical water content of $Nb_2O_3(SO_4)_2 \cdot \frac{1}{4}H_2O$ is 1.1 wt%. The continuous mass loss of 3 wt% up to ≈ 500°C agrees reasonable well with loss of water. The higher experimental value can be explained by a remaining impurity of sulfur in the sample. The theoretical mass loss for the decomposition of $Nb_2O_3(SO_4)_2$ into Nb_2O_5 by the loss of two SO_3 is 37.6 wt%. This fits well to the 35 wt% large drop in the TG curve beginning at ≈ 500°C and ending at ≈ 800°C. The color of the sample had changed from blue to light yellow after this drop.

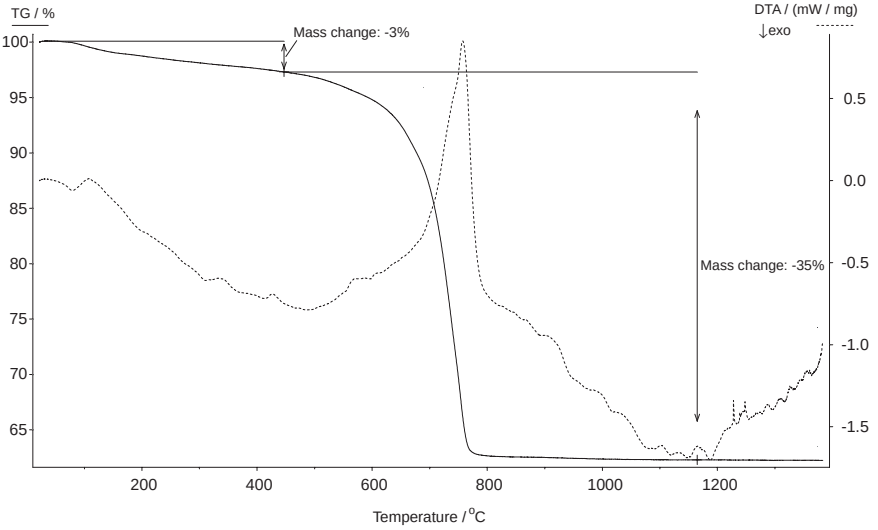

Fig. 8. TGA/DTA diagram of the decomposition of $Nb_2O_3(SO_4)_2 \cdot \frac{1}{4}H_2O$ in air atmosphere (heating rate 10 K/min).

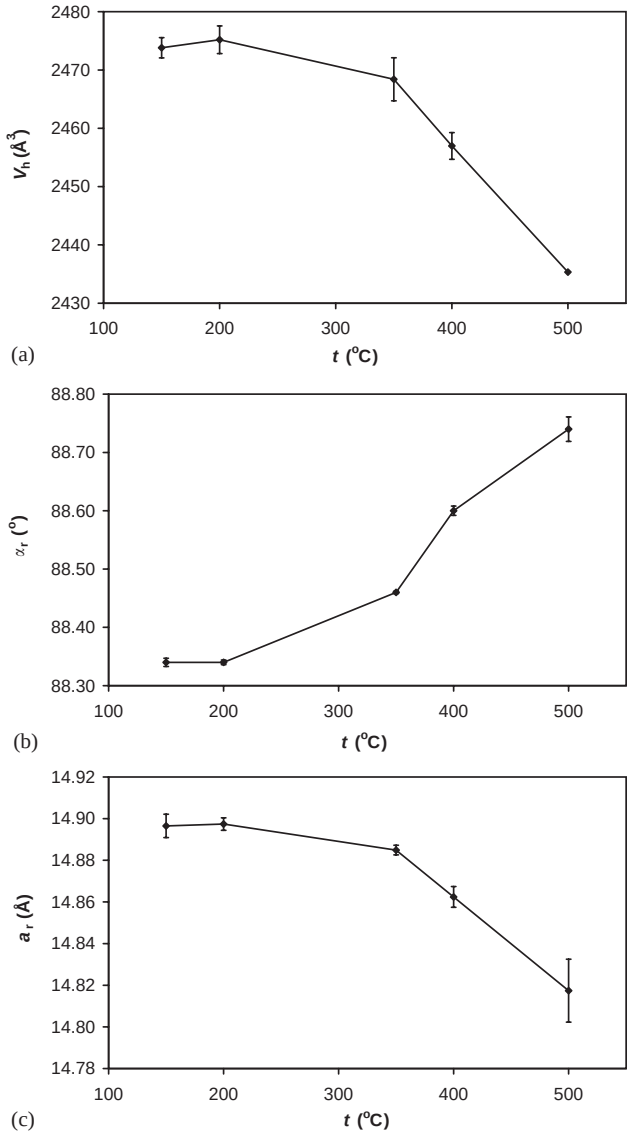

Fig. 9. (a) Cell volume of $Nb_2O_3(SO_4)_2 \cdot \frac{1}{4}H_2O$ (hexagonal setting) as function of the annealing temperature. (b) Rhombohedral angle of the unconventional face centred rhombohedral cell as function of annealing temperature. (c) Cell axis of the unconventional face centred rhombohedral cell as function of annealing temperature. Error bars show the standard deviations of the values.

The rhombohedral angle of the unconventional face centered rhombohedral cell increases as a function of increasing annealing temperature, i.e., the angle approaches the cubic value, as shown in Fig. 9. The diffraction pattern of $Nb_2O_3(SO_4)_2$ heated at 400°C for 508 h showed no extra reflections, while two extra reflections were observed for the sample heated at 500°C for 22 h. About half of the diffracted intensity in the diffraction pattern from a sample annealed at 550°C for 67 h originated from phases different from $Nb_2O_3(SO_4)_2$. The cell parameter of the sample annealed at 350°C remained unchanged after the 7 months long water treatment.

4. Discussion and conclusions

Although the synthesis route is different, it is most probable that the title compound is identical to the blue $Nb_2O_3(SO_4)_2$ reported by Land and Sanchez-Caldas [21]. It has previously been suggested that $Nb_2O_3(SO_4)_2$ could be a pyrosulfate, since the compound also can be written $Nb_2O_4(S_2O_7)$ [21]. The present study shows that this is not the case. The structure of the title compound is very dissimilar to previously known oxysulfates. Its three-dimensional local network of eight apex-sharing niobate octahedra is unique. Similar three-dimensional local networks are only found in cluster compounds, but there these networks are not covalently interconnected with each other. Both magnetization measurements and bond valence calculations clearly show that the Nb atoms are in the +V oxidation state. The water molecules are at least partly the cause for the rhombohedral distortion, based on the fact that the compound approaches cubic symmetry as a function of decreasing water content. During the water loss, the compound changes color into whitish pale yellow. This suggests that the blue color is related to the water molecules in the structure. The water is continuously and irreversibly lost up to approximately 500°C, where the whole structure starts to slowly break down. The structure is stable at least to 400°C. At 550°C the decomposition becomes rapid.

Acknowledgments

We would like to thank the staff of the ESRF ID31 beam line, especially Andy Fitch for useful discussions and technical assistance during the experiment and also Monica Dapiaggi and Walter Tiano for help during the data collection. We also thank the staff of Studsvik Neutron Facility for the neutron measurement and Rainer Niewa for the TGA/DTA measurement.

References

[1] Y.G. Goroshchenko, J. Inorg. Chem. USSR English Trans. 1 (1956) 24 (English Trans).
[2] P.J. Squattrito, P.R. Rudolf, A. Clearfield, Inorg. Chem. 26 (1987) 4240.
[3] A. Mueller, J. Doering, Z. Anorg. Allg. Chem. 595 (1991) 251.
[4] P. Kierkegaard, J.M. Longo, B.O. Marinder, Acta Chem. Scand. 19 (1965) 763.
[5] S. Boghosian, K.M. Eriksen, R. Fehrmann, K. Nielsen, Acta Chem. Scand. 49 (1995) 703.
[6] J.M. Longo, R.J. Arnott, J. Sol. State Chem. 1 (1970) 394.
[7] B.M. Gatehouse, S.N. Platts, T.B. Williams, Acta Crystallogr. 49 (1993) 428.
[8] I.E. Grey, R. Stranger, J. Sol. State Chem. 101 (1992) 331.
[9] M.A.K. Ahmed, H. Fjellvag, A. Kjekshus, Acta Chem. Scand. 50 (1996) 275.

[10] G. Lundgren, Arkiv Kemi. 10 (1956) 397.
[11] K. Richter, R. Mattes, Z. Anorg. Allg. Chem. 611 (1992) 158.
[12] R. Fehrmann, S. Boghosian, G.N. Papatheodorou, K. Nielsen, R.W. Berg, N.J. Bjerrum, Inorg. Chem. 28 (1989) 1847.
[13] M. Tachez, F.R. Theobald, Acta Crystallogr. B 37 (1981) 1978.
[14] J.M. Longo, P. Kierkegaard, Acta Chem. Scand. 20 (1966) 72.
[15] U. Kaiser, G. Schmidt, R. Glaum, R. Gruehn, Z. Anorg. Allg. Chem. 607 (1992) 113.
[16] A. Leclaire, H. Chahboun, D. Groult, B. Raveau, Z. Kristallogr. 177 (1986) 277.
[17] V.P. Nicolaev, G.G. Sadikov, A.V. Lavrov, M.A. Porai-Koshits, Izvestiya Akademii Nauk SSSR, Neorg. Mater. 22 (1986) 1364.
[18] J.J. Zah-Letho, A. Jouanneaux, A.N. Fitch, A. Verbaere, M. Tournoux, Eur. J. Sol. State Inorg. Chem. 29 (1992) 1309.
[19] D.L. Serra, S.-J. Hwu, Acta Crystallogr. C 48 (1992) 733.
[20] A. Leclaire, M.M. Borel, A. Grandin, B. Raveau, Acta Crystallogr. C 45 (1989) 699.
[21] J.E. Land, J.R. Sanchez-Caldas, J. Less-Common Metals 13 (1967) 233.
[22] A. Altomare, M.C. Burla, G. Cascarano, C. Giacovazzo, A. Guagliardi, A.G.G. Moliterni, G.J. Polidori, Appl. Crystallogr. 28 (1995) 842.
[23] A. Altomare, G. Cascarano, C. Giacovazzo, A. Guagliardi, M.C. Burla, G. Polidori, M. Camalli, J. Appl. Cryst. 27 (1994) 435.
[24] J. Laugier, B. Bochu, Cellref v.3, Laboratoire des Materiaux et du Génie Physique de l'Ecole Supérieure de Physique de Grenoble, 2003.
[25] A.C. Larson, R.B. von Dreele, GSAS, Los Alamos National Laboratory, NM 87545, USA, 1995.
[26] M. Nespolo, G. Ferraris, H. Ohasi, Acta Crystallogr. B 55 (1999) 902.
[27] I.D. Brown, D. Altermatt, Acta Crystallogr. B 41 (1985) 244.